

Absence of Localization in Two-Dimensional Clifford Circuits

Tom Farshi^{1,2,3} , Jonas Richter^{2,4,5} , Daniele Toniolo^{1,2} , Arijeet Pal² , and Lluís Masanes^{1,6,*} 

¹*Department of Computer Science, University College London, Gower Street, London WC1E 6BT, United Kingdom*


²*Department of Physics and Astronomy, University College London, Gower Street, London WC1E 6BT, United Kingdom*

³*School of Mathematics, University of Bristol, Queens Road, Bristol BS8 1QU, United Kingdom*

⁴*Department of Physics, Stanford University, Stanford, California 94305-4013, USA*

⁵*Institut für Theoretische Physik, Leibniz Universität Hannover, Appelstraße 2, 30167 Hannover, Germany*

⁶*London Centre for Nanotechnology, University College London, Gordon Street, London WC1H 0AH, United Kingdom*

 (Received 31 October 2022; revised 14 February 2023; accepted 1 May 2023; published 6 July 2023)

We analyze a Floquet circuit with random Clifford gates in one and two spatial dimensions. By using random graphs and methods from percolation theory, we prove in the two-dimensional (2D) setting that some local operators grow at a ballistic rate, which implies the absence of localization. In contrast, the one-dimensional model displays a strong form of localization, characterized by the emergence of left- and right-blocking walls in random locations. We provide additional insights by complementing our analytical results with numerical simulations of operator spreading and entanglement growth, which show the absence (presence) of localization in two dimensions (one dimension). Furthermore, we unveil how the spectral form factor of the Floquet unitary in 2D circuits behaves like that of quasifree fermions with chaotic single-particle dynamics, with an exponential ramp that persists up to times scaling linearly with the size of the system. Our work sheds light on the nature of disordered Floquet Clifford dynamics and their relationship to fully chaotic quantum dynamics.

DOI: [10.1103/PRXQuantum.4.030302](https://doi.org/10.1103/PRXQuantum.4.030302)

I. INTRODUCTION

An understanding of the dynamics of quantum many-body systems far from equilibrium is of fundamental importance for preparing and controlling quantum states of matter [1]. The universal dynamical behavior provides signatures of novel quantum phases of matter and their underlying patterns of quantum information. The study of the dynamics of quantum many-body systems is notoriously challenging due to the exponential growth of the Hilbert space. In recent years, simulation of the dynamics in a quantum circuit architecture has opened up new directions for probing quantum chaos, hydrodynamics, and nonequilibrium phases of matter [2–9]. These phenomena are particularly suitable for quantum simulation on noisy intermediate-scale quantum (NISQ) devices and have been studied on state-of-the-art physical platforms.

Novel quantum many-body phenomena can be realized in these experiments, providing a test bed for the theoretical ideas with potential applications in protecting and processing quantum information.

The dynamics in circuit models is encoded in the form of k -local unitary gates acting on qubits. The geometry of the gates and their symmetries provide access to a wide range of model phenomena that are analytically tractable and can be approximated efficiently. Due to their tunability and control, circuit models provide minimal models for complex quantum phenomena, including systems with kinetic constraints [10,11], dual-unitary structure [12,13], periodic dynamics [14], and long-range interactions [15]. Notably, quantum circuits with random gates have provided a powerful framework to strive for a quantum computational advantage [16] as well as to study quantum information scrambling on existing quantum hardware [17].

The vast majority of many-body quantum systems are ergodic and relax to thermal equilibrium under unitary time evolution [18,19]. Exceptions to this generic thermalizing behavior include integrable models [20], which possess an extensive set of conservation laws, as well as models exhibiting localization [21,22]. Localization can arise in systems with sufficiently strong disorder and one of its

*l.masanes@ucl.ac.uk

Published by the American Physical Society under the terms of the [Creative Commons Attribution 4.0 International](https://creativecommons.org/licenses/by/4.0/) license. Further distribution of this work must maintain attribution to the author(s) and the published article's title, journal citation, and DOI.

signatures is the slow growth of any initially local operator when evolving in the Heisenberg picture. In a quantum circuit, localization in terms of operator growth can be of single-particle type, where the support of any initially local operator remains confined in a finite region for all times [23,24] as, e.g., realized in lattice models of noninteracting fermions with random on-site potential [25] and for the corresponding mapping to spin systems [26,27]. For a typical realization of our circuit in one dimension, this definition takes into account the appearance of walls that block the spread of any operator, as illustrated in Fig. 1(a). On the other hand, many-body localization (MBL) exhibits the growth of support of a local operator as the logarithm of time [28]. In particular, the loglike growth of entanglement entropy in time [29–31] tells these systems apart from the Anderson-type localized as defined below in Definition 1. In one-dimensional (1D) systems, a many-body localized phase with an extensive set of exponentially localized integrals of motion might exist at sufficiently strong disorder [32]. However, the asymptotic existence of this MBL phase in the thermodynamic limit is still under active debate, as localization has recently been found to be unstable even at rather large values of disorder [33–37]. Moreover, in higher dimensions, analytical arguments and numerical calculations suggest that MBL is unstable [38–43].

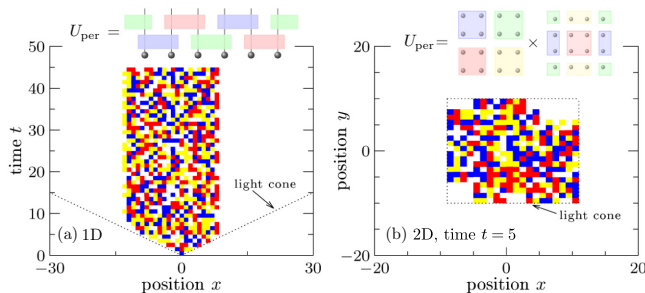


FIG. 1. Localization and its absence in Floquet Clifford circuits. A local operator σ_x acting nontrivially only on a single site evolves according to a time-periodic Clifford circuit in (a) 1D and (b) 2D, $t = 5$. In 1D, the Floquet unitary U_{per} consists of a brickwork pattern of two-qubit gates, while in 2D it consists of two layers of four-qubit gates (cf. Fig. 2). The color plot encodes the local matrices of the time-evolved operator string $U(t)\sigma_x U^\dagger(t)$ according to $\mathbb{1}$ (white), σ_x (blue), σ_y (red), or σ_z (yellow). The data are shown for a single random realization of the Clifford gates. For better visualization of the 2D data, we focus in (b) on a single point in time, $t = 5$, where the light-cone boundary (dotted square) is of size 20×20 (cf. Definition 2). As proven in Ref. [14], the 1D circuit exhibits localization due to the emergence of left- and right-sided walls that confine the evolution at all times. This confinement affects all (not necessarily Pauli) operators with support between the two walls. Inside the confined region, the evolution looks ergodic. In contrast, in 2D, localization is absent, as can be seen from the fact that parts of the operator grow with the light-cone speed.

Disorder in quantum circuit models can be introduced in space and time where the gates are chosen at random. Random unitary dynamics without any symmetries or constraints lead to complete mixing [3,4,44,45], while certain time-periodic circuits can exhibit nonergodic dynamics [14,46]. There are also various forms of kinetically constrained random circuits, akin to fractonic models, that exhibit localization [47,48]. In this work, we shed light on the role of dimensionality on localization in random Floquet Clifford circuits. Floquet circuits have been extensively studied [46,49–53] and have provided key insights into the properties of periodically driven quantum systems [54]. They have been essential to rigorously demonstrate the occurrence of chaos and random-matrix behavior in isolated quantum systems [49,52] and, in combination with disorder and many-body localization, they can host exotic nonequilibrium phases of matter with no equilibrium counterpart [55,56]. Moreover, certain circuits with dual-unitary structure allow for a controlled tuning between ergodic and nonergodic dynamics [12,13]. In this work, we analytically and numerically study the absence of localization in two-dimensional (2D) Clifford circuits and characterize the integrable nature of chaos using measures of operator growth and spectral form factor (SFF). Moreover, we numerically contrast the 2D against the 1D case, showing for the latter localization at the dynamical level.

From a quantum information perspective, the Clifford group plays a key role in fault-tolerant quantum computing and randomized benchmarking [57–59]. Recently, random circuits consisting of Clifford gates have provided useful insights into quantum many-body physics [2,14,60–62] due to their efficient simulability on classical computers despite the generation of extensive amounts of entanglement. This efficient simulability of Clifford dynamics can also be understood in terms of a phase-space representation analogous to that of quasifree bosons and fermions, with the dimension of the phase space being exponentially smaller than the Hilbert space (see appendix A of Ref. [14] and Refs. [63,64]). Yet, Clifford circuits form unitary designs [65–67] such that circuit averages of certain relevant quantities can exactly reproduce Haar averages over the full unitary group. Despite their simplicity, Clifford circuits can thus prove useful to gain insights into some aspects of the dynamics of more generic quantum systems, including the build-up of out-of-time-ordered correlators and the growth of entanglement [3,4].

In addition, as we demonstrate, the Clifford circuits studied in this paper are to some extent tractable analytically by a suitable mapping to directed graphs. It is known that random time-dependent (i.e., annealed disorder) cellular automata can be analyzed using directed-percolation theory [68,69] and that Clifford circuits can be represented as cellular automata. However, the circuits considered by us are not random in time, they have quench disorder, and hence, they cannot in general be solved with directed

graphs. Nevertheless, as we show below, in order to probe their behavior, we only need to analyze the dynamics at the edge of the light cone. Moreover, at the light-cone edge, spatial disorder is equivalent to time disorder, producing an effectively annealed dynamics, which can be analyzed using percolation theory.

The hybrid nature of Clifford circuits between integrable and chaotic systems is also reflected in the emergence of ergodicity and localization. On the one hand, it has been shown in Ref. [14] that Floquet Clifford circuits exhibit Anderson-type localization in 1D [cf. Fig. 1(a) and Definition 1]. On the other, we prove here, and numerically show [cf. Fig. 1(b)], as a main result, that in 2D, some operators always grow at a ballistic rate, such that the model does not localize, despite having strong disorder, contrasting the phenomenon in 1D. We also provide numerical evidence that the ballistic growth happens for almost all local operators. Moreover, the absence of localization in our time-periodic 2D circuit model differs from the behavior of disordered free-fermion models, which show Anderson localization for arbitrarily weak disorder in 2D [70–72].

We elucidate further aspects of the Floquet Clifford dynamics by complementing our analytical results with numerical simulations, where we demonstrate that operator spreading is exponentially suppressed in 1D, reminiscent of the exponential dynamical-localization of the wave function in Anderson insulators. On the contrary, we find that operator spreading in 2D occurs ballistically with light-speed velocity and that the interior of the light cone becomes fully scrambled and featureless. These findings are substantiated by the temporal build-up of entanglement, which is bounded and system-size independent in 1D, whereas it grows linearly and saturates toward extensive values in 2D. Finally, we also study the SFF of the Floquet Clifford circuit, which is a key quantity to diagnose the emergence of quantum chaos. We show that the SFF is similar to that of free fermions, the associated single-particle dynamics of which are chaotic. Specifically, we find that, in the 2D model, the SFF exhibits an exponential ramp at early times that persists up to a time that scales linearly with the size of the system, suggesting that ergodicity in the case of Clifford dynamics should be understood with respect to the exponentially smaller phase space.

Our work provides a comprehensive picture of localization and chaos in disordered Floquet Clifford quantum circuits, in terms of directed percolation, at the light cone, and information spreading in classical cellular automata. An understanding of nonequilibrium quantum many-body states in Clifford circuits provides an important starting point for studying the phenomena in generic conditions. It can serve as a useful benchmark for identifying quantum effects of simulation in noisy quantum devices. The relevance of Clifford circuits for quantum error correction

can also provide valuable insights into combining error-correction protocols with quantum simulation.

The rest of this paper is structured as follows. Section II A contains a description of the model, including the definition of Clifford unitaries, which are the building blocks of this quantum circuit. Section II B contains the main result of our work, Theorem 1, together with a discussion of its significance, as well as its numerical demonstration in Sec. II C. In Sec. II D, we numerically study the SFF of Floquet Clifford unitaries, which supports our observation of localization in 1D (see also Ref. [14]) and ergodic dynamics in 2D. We also provide a rigorous lower bound on the time-averaged SFF. Section III contains the proof of Theorem 1, which uses random graphs and methods reminiscent of those of percolation theory. Eventually, in Sec. IV, we provide a discussion about the fact that Clifford dynamics appears to share properties of integrable systems and chaotic systems. Section V summarizes the results of this work and provides some outlook. The Appendix provides the relation between the localization length and the average position of a blocking wall in the dynamics of the 1D model.

II. RESULTS

A. Description of the model

Consider an infinite 2D square lattice with sites labeled by $(x, y) \in \mathbb{Z}^2$. At each site, there is a spin-1/2 particle, or qubit, which has Hilbert space \mathbb{C}^2 . The dynamics of the system is time periodic, with the period being one unit of time. Hence, at integer times $t \in \mathbb{Z}$, the evolution operator can be written as $U(t) = (U_{\text{per}})^t$. The unitary U_{per} that describes the dynamics of a single period has the form

$$U_{\text{per}} = \left(\bigotimes_{x,y \text{ odd}} W_{(x,y)} \right) \left(\bigotimes_{x,y \text{ even}} W_{(x,y)} \right), \quad (1)$$

where, for any $(x, y) \in \mathbb{Z}^2$, the local unitary $W_{(x,y)}$ acts on the four sites (x, y) , $(x + 1, y)$, $(x, y + 1)$, and $(x + 1, y + 1)$. In Eq. (1), $(x, y \text{ odd})$ means that both x and y are odd: analogously, $(x, y \text{ even})$ means that both x and y are even. In the dynamics described by Eq. (1), each time period decomposes into two half time steps, which are illustrated in Fig. 2. This quantum circuit with local interactions is an example of a quantum cellular automaton (QCA) [11, 73–75]. The evolution operator $U(t)$ can also be generated by a time-periodic Hamiltonian $H(t)$ with local interactions

$$U(t) = \mathcal{T} e^{-i \int_0^t d\tau H(\tau)}, \quad (2)$$

where \mathcal{T} denotes a time-ordered exponential. This type of dynamics is called Floquet dynamics [54].

The disorder of the system is represented by the fact that each local unitary $W_{(x,y)}$ is sampled independently from

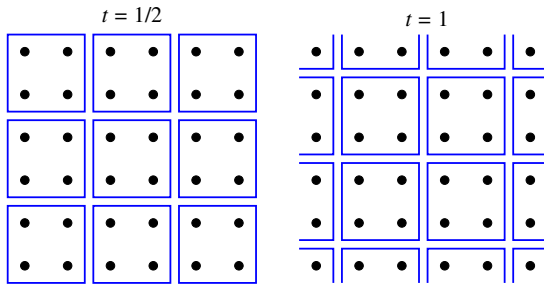


FIG. 2. The local dynamics. This figure represents the two layers of local unitaries generating the dynamics of a time period U_{per} . Each black dot represents a qubit and each blue square represents a four-qubit unitary $W_{(x,y)}$.

the uniform distribution over the four-qubit Clifford group. A unitary W is Clifford if it maps any product of Pauli sigma matrices to another product of Pauli sigma matrices [63,76]. An example of Clifford unitary W acting on $\mathbb{C}^2 \otimes \mathbb{C}^2$ is

$$W(\sigma_x \otimes \mathbb{1})W^\dagger = \sigma_z \otimes \sigma_x, \quad (3)$$

$$W(\sigma_z \otimes \mathbb{1})W^\dagger = \mathbb{1} \otimes \sigma_z, \quad (4)$$

$$W(\mathbb{1} \otimes \sigma_x)W^\dagger = \sigma_z \otimes \mathbb{1}, \quad (5)$$

$$W(\mathbb{1} \otimes \sigma_z)W^\dagger = \sigma_x \otimes \sigma_z. \quad (6)$$

It can be seen that these four identities fully specify W up to a global phase. Clearly, having random Clifford unitaries in neighboring unit cells is a somewhat different type of disorder than the one usually considered in the study of localization (e.g., random on-site magnetic fields in spin-chain models [21,22]). For instance, apart from the fact that the unitaries are drawn independently, it is not immediately obvious how to quantify the strength of the disorder in the random-circuit model.

In summary, we study the typical behavior of an ensemble of models. Note that while the statistics defining the model is translation invariant, typical instances are not. This approach is standard in the study of disorder and localization [23]. We also have to mention that the Floquet Clifford circuit described in Eq. (1) and Fig. 2 is a straightforward 2D version of the 1D model considered in Ref. [14]. Remarkably, in Ref. [14], it has been proven that the 1D Floquet model with two-qubit Clifford gates acting in a brickwork pattern supports Anderson-type localization. More specifically, local operators remain confined to a finite region in space during the time evolution due to the emergence of left- and right-sided walls [cf. Fig. 1(a)] that confine the operator spreading at all times (see also Ref. [77]). Here, we prove that this kind of localization is absent in the 2D model [cf. Fig. 1(b)]. In this context, let us note that this absence of localization in 2D is in contrast

to the results of Ref. [77], which has studied similar Floquet Clifford circuits hosting a localization-delocalization transition in 2D. However, while Ref. [77] has considered a drastically reduced gate set (only two different two-qubit Clifford elements), our circuits are more general, with gates being drawn at random from the full Clifford group.

One difference between the 1D model [Fig. 1(a)] and the 2D model [Fig. 1(b)] is that in the former case the gates are sampled from the two-qubit Clifford group \mathcal{C}_2 , while in the latter case they are sampled from the four-qubit Clifford group \mathcal{C}_4 . Both contain a finite number of distinct elements but their dimensions differ substantially, i.e., $|\mathcal{C}_2| = 11\,520$ and $|\mathcal{C}_4| \approx 1.2 \times 10^{13}$ [78].

In the following, our analytical arguments are focused on the 2D model of Eq. (1) and we refer the interested reader to Ref. [14] for the proof of localization in 1D. However, in order to provide a concrete comparison of their properties, we present numerical results of operator spreading and entanglement growth (Sec. II C), as well as simulations of the SFF (Sec. II D), for both 1D and 2D Floquet Clifford circuits.

B. Absence of localization

Many-body lattice systems display localization when the Lieb-Robinson velocity vanishes. Next, we provide a definition of Anderson-type localization based on Ref. [26].

Definition 1.—Let $O^H(t) = e^{iHt} O e^{-iHt}$ be the evolution in the Heisenberg picture of a local observable O with support at the origin of the lattice and let $O_l^H(t)$ be the restriction of $O^H(t)$ onto the ball of radius $l > 0$ around the origin. A system displays *Anderson-type localization* if there are parameters $c, \mu > 0$ such that

$$\mathbb{E}_H \sup_t \|O_l^H(t) - O^H(t)\|_\infty \leq c e^{-\frac{l}{\mu}}, \quad (7)$$

for all $l > 0$. (The operator norm $\|A\|_\infty$ is the spectral radius of A , which for finite systems is the largest singular value of A .)

Note that the left-hand side of Eq. (7) involves an average over all realizations of the Hamiltonian H , which usually correspond to different realizations of a random potential. In the case of QCAs or Floquet systems, the average is taken over the single-period unitary U_{per} characterizing the dynamics $O(t) = U_{\text{per}}^{-t} H U_{\text{per}}^t$. In particular, in quantum circuits, the average runs over all realizations of the circuit. The above definition implies that if a system has dynamics such that a local operator grows at a linear rate (ballistically) in some direction, then we can conclude that there is no localization of any type. With this in mind, we make the following definitions.

Definition 2.—The *light cone* is the largest support that a single-site operator at $t = 0$ could have at each future time t when we maximize over instances of the dynamics (see

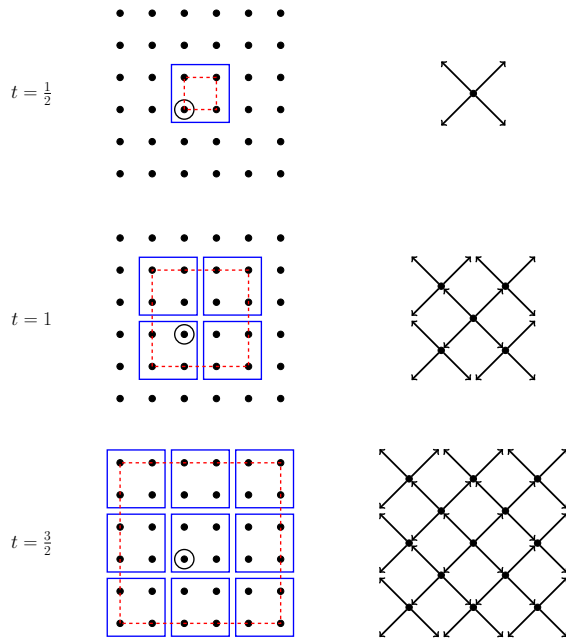


FIG. 3. Light-cone boundary growth. The left column shows the light cone and its boundary at times $t \in \{1/2, 1, 3/2\}$ of an operator acting on the encircled site at $t = 0$. The black dots represent sites, the blue squares represent four-qubit unitaries, and the red dashed line is the light-cone boundary. The right column shows the segment of the directed graph G that describes the growth history of the boundary up to the corresponding time t . Each vertex in G represents a unitary and each arrow represents a qubit at a particular time t . The arrows that do not point to any vertex represent the qubits of the boundary at time t .

Fig. 3). At each time t , the *boundary* of the light cone consists of the outer qubits contained in the light cone, which form a square of side $4t$.

The approximate shape of the light cone is a four-sided pyramid, the apex of which is the site where the initial operator is supported. The surface of this pyramid is the boundary of the light cone. In general, an operator may not have full support inside the light cone, because it acts as the identity at some sites at particular times (see Fig. 4). However, despite not having full support, an operator may grow at maximal speed, as defined next.

Definition 3.—A model has *light-speed operator growth* if there is a single-site operator the evolution of which has nontrivial support (is nonidentity) on the boundary of the light cone at all future times $t = 1, 2, 3, \dots$ (see Fig. 4).

Light-speed operator growth implies the absence of localization. However, not having light-speed operator growth does not imply localization. For example, ballistic growth at a rate smaller than unity is not localization. Also, diffusive dynamics, where the diameter of the support of an operator grows as the square root of time, is not localization. In what follows, we introduce the main result

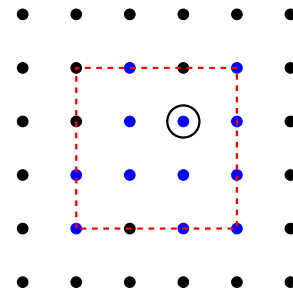


FIG. 4. Light-speed growth. In this example, an operator located at the circled site at time $t = 0$ evolves into an operator with support on the blue sites at time $t = 1$. Since some of these blue sites are at the light-cone boundary (red dashed line), this operator enjoys light-speed growth (at least up to time $t = 1$).

of this work, which establishes the absence of localization in our model.

Theorem 1.—Consider a Pauli operator that differs from the identity only on a single site at $t = 0$. With probability at least 0.44, the time evolution of this operator generated by the random dynamics given in Eq. (1) is nonidentity on some sites of the boundary of the light cone at all times $t \in \{1/2, 1, 3/2, 2, 5/2, \dots\}$.

That is, with probability 0.44, a particular Pauli operator at a particular site enjoys light-speed growth. Our numerical simulations strongly suggest that this happens for a fraction much larger than 0.44. Non-Pauli operators are more prone to light-speed growth, because they have more than one term when expressed in the Pauli basis and hence there is a greater likelihood that at least one term has light-speed growth.

Before turning to the formal proof of Theorem 1 in Sec. III, we now provide numerical support for the presence (absence) of localization in 1D (2D) random Floquet Clifford circuits. In particular, let us note that while some aspects of the Clifford dynamics can be treated analytically (cf. Sec. III), others are accessible only by numerical means.

C. Numerical analysis of Floquet Clifford circuits

1. Simulating Clifford circuits

Clifford circuits can be efficiently simulated on classical computers by exploiting the stabilizer formalism [63,64]. More specifically, a stabilizer state $|\psi\rangle$ on L qubits can be uniquely defined by L operators \mathcal{P}_i according to $\mathcal{P}_i |\psi\rangle = |\psi\rangle$, where the \mathcal{P}_i are L -qubit Pauli strings. Instead of keeping track of the time evolution of the quantum state directly, $|\psi\rangle \rightarrow U(t) |\psi\rangle$, it is then useful to consider the evolution of the operators, $\mathcal{P}_i \rightarrow U(t)\mathcal{P}_i U^\dagger(t)$. The latter can be done efficiently if $U(t)$ consists solely of Clifford gates that map single Pauli strings to other single Pauli strings [cf. Eq. (3)], in stark contrast to more general

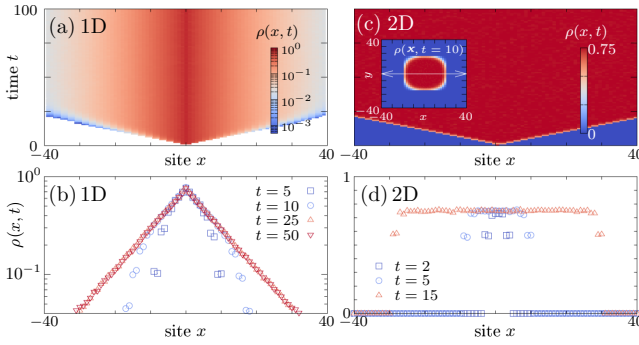


FIG. 5. Operator spreading. Circuit-averaged $\rho(x, t)$ in (a),(b) refers to the 1D system and (c),(d) refers to the 2D system. The data are obtained by time evolving an initially local operator σ_x located at the origin and averaging over approximately 10^4 random-circuit realizations. Panels (b) and (d) show cuts of the data in (a) and (c) at fixed times t . For the better visualization of the 2D data, (c) shows $\rho(x, t)$ along a cut with $y = 0$ [as indicated by the white arrow in the inset of (c), which depicts the full 2D data at $t = 10$]. While in 1D, the operator becomes exponentially localized, with $\rho(x, t) \propto e^{-x/\mu}$ and $\mu \approx 10.4$, the operator grows with light speed in 2D with a maximally scrambled light-cone interior, as indicated by $\rho(x, t) \approx 3/4$.

quantum evolution, which would yield superpositions of multiple Pauli strings. More specifically, the L stabilizers \mathcal{P}_i can be encoded in a $L \times 2L$ binary matrix, also called the *stabilizer tableau*, the values of which are updated suitably upon the application of a Clifford gate. As a consequence, the time and memory requirements scale only polynomially with the number of qubits (for further details, see Ref. [63]). In fact, time evolving the entire stabilizer tableau of a state $|\psi\rangle$ will be necessary here only for calculating the entanglement entropy in Fig. 6, whereas the analysis of operator spreading (Figs. 1 and 5) and of the SFF below (Fig. 7) requires the evolution of single (or, in

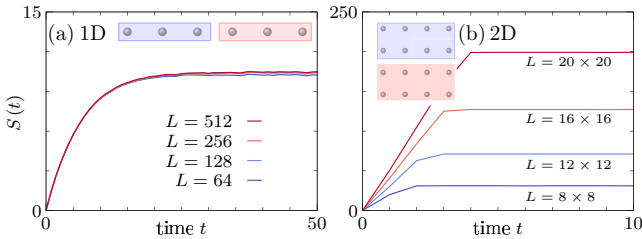


FIG. 6. Entanglement growth. The half-system (cf. sketches) entanglement entropy $S(t)$ under Floquet Clifford evolution for different system sizes L in (a) 1D and (b) 2D. In 1D, $S(t)$ approaches an almost system-size independent long-time value. In 2D, $S(t)$ saturates toward the maximally achievable value $L/2$. [Note the different scales of the y axis in (a) and (b).] The data are averaged over approximately 10^3 random-circuit realizations.

the case of the SFF, a specific set of) operators. Eventually, we note that there exist various efficient algorithms to generate random elements of the Clifford group [78,79]. Here, we follow the approach of Ref. [80], which we use to sample uniformly from \mathcal{C}_2 (\mathcal{C}_4) in our simulations of 1D (2D) circuit geometries. Except for Fig. 1, we then present results that are averaged over a sufficient number of random-circuit realizations.

2. Operator spreading

Figure 1(a) demonstrates the occurrence of localization in 1D Floquet Clifford circuits. Specifically, considering $\mathcal{O}(0) = \mathbb{1} \otimes \cdots \otimes \mathbb{1} \otimes \sigma_x \otimes \mathbb{1} \otimes \cdots \otimes \mathbb{1}$, which differs from the identity only at one site, Fig. 1 shows its time evolution $\mathcal{O}(t) = U(t)\mathcal{O}(0)U^\dagger(t)$ for a single random-circuit realization. While the operator grows at light speed at short times, this growth eventually stops in 1D due to the emergence of left- and right-blocking walls, leading to the Anderson-type localization behavior proven in Ref. [14]. In contrast, this kind of localization is absent in the 2D circuit [Fig. 1(b)], where we find that at least some parts of the time-evolved operator grow with light speed, that is, they act nontrivially on the light-cone boundary at all times.

In order to study this operator spreading in more detail, let $\mathcal{O}_x(t)$ denote the local Pauli matrix at the x th position of the time-evolved operator. (For example, given a two-qubit system and $\mathcal{O}(t) = \sigma_x \otimes \sigma_z$, we might have $\mathcal{O}_1(t) = \sigma_x$ and $\mathcal{O}_2(t) = \sigma_z$.) We then define the quantity $\rho(x, t)$, with

$$\rho(x, t) = \begin{cases} 1, & \text{if } \mathcal{O}_x(t) = \sigma_x, \sigma_y, \sigma_z, \\ 0, & \text{if } \mathcal{O}_x(t) = \mathbb{1}. \end{cases} \quad (8)$$

In Fig. 5, we show the *circuit-averaged* dynamics of $\rho(x, t)$ for 1D and 2D circuits. (Note that here we refrain from introducing another symbol for the average.) On the one hand, in the case of 1D circuits [Figs. 5(a) and 5(b)], we find that most of the support of the operator remains close to the origin. More specifically, we find that the operator spreading is exponentially localized, with $\rho(x, t) \propto e^{-x/\mu}$, $\mu \approx 10.4$, and becomes essentially stationary at long times, as can be seen by comparing the cuts of $\rho(x, t)$ at times $t = 25$ and $t = 50$ in Fig. 5(b).

On the other hand, the situation is clearly different in 2D [Figs. 5(c) and 5(d)]. In this case, we find that $\rho(x, t)$ is essentially featureless inside the light cone with $\rho(x, t) \approx 3/4$, with a sharp drop to $\rho(x, t) \rightarrow 0$ outside the light cone. Note that for better visualization, the data in Fig. 5(c) are shown for a cut at $y = 0$ of the original 2D data [cf. the inset in Fig. 5(c)]. Importantly, the circuit-averaged value $\rho(x, t) \approx 3/4$ indicates maximally scrambling dynamics. Namely, given the definition in Eq. (8) of $\rho(x, t)$, this value indicates that the matrices $\sigma_x, \sigma_y, \sigma_z$, and $\mathbb{1}$ locally occur all with equal probability.

It is in principle conceivable that there exist rare instances of random gate configurations such that the operator spreading also becomes localized in 2D. In practice, however, we do not observe any such localized instances and, in particular, there are no notable signatures in the circuit-averaged behavior of $\rho(x, t)$ in Figs. 5(c) and 5(d).

3. Entanglement dynamics

To proceed, we now turn to the build-up of entanglement $S(t)$ between two parts A and B of the system, starting from an initially unentangled product state $|\uparrow\rangle^{\otimes L}$ stabilized by σ_z everywhere. Within the stabilizer formalism, $S(t)$ can be efficiently simulated based on the collective evolution of all L operators \mathcal{P}_i that define $|\psi\rangle$ [2,81]. Note that the entanglement dynamics in Clifford circuits is somewhat special since, given the reduced density matrix $\rho_A(t) = \text{tr}_B |\psi(t)\rangle\langle\psi(t)|$, $\rho_A(t)$ will exhibit a flat eigenvalue spectrum such that all its Rényi entropies are equivalent [82]. Nevertheless, Clifford circuits can support extensive amounts of entanglement and the dynamics of $S(t)$ are often found to mimic the properties of more generic quantum evolutions [15,60].

In Fig. 6, we show $S(t)$ for half-system bipartitions in 1D and 2D Floquet Clifford circuits with various system sizes L . The dynamics of $S(t)$ substantiate our previous observation of localization in 1D and ergodic behavior in 2D. Specifically, we find that $S(t)$ saturates toward a rather small and essentially L -independent long-time value $S(t \rightarrow \infty) \approx 10$ in 1D [Fig. 6(a)]. This emphasizes that the localization length in 1D is distinctly shorter than the full system size and that a local operator can only explore a small part of the system [cf. Fig. 1(a)]. In contrast, in 2D [Fig. 6(b)], we find that $S(t)$ exhibits a pronounced linear increase at short times, well known from other random-circuit models and chaotic quantum systems. Moreover, at longer times, $S(t)$ saturates toward an extensive long-time value $S(t \rightarrow \infty) \approx L/2$, which is the maximally achievable value for a system of size L . This volume-law scaling of $S(t)$ highlights the absence of localization in 2D Floquet Clifford circuits.

D. Spectral form factor

1. Definition and general remarks

To provide further insights into the nature of Floquet Clifford circuits we now turn to the SFF. The SFF of an ensemble of unitaries \mathcal{U} is defined as

$$K(t) = \langle |\text{tr } U^t|^2 \rangle, \quad (9)$$

where t takes integer values and the brackets $\langle \dots \rangle$ denote the ensemble average over all $U \in \mathcal{U}$. The SFF probes the statistical properties of the spectrum of randomly sampled

unitaries in \mathcal{U} . In particular, the Fourier transform

$$\tilde{K}(\omega) = \frac{1}{\pi} \sum_{t=1}^{\infty} K(t) \cos(\omega t) \quad (10)$$

is the probability that a random $U \in \mathcal{U}$ has two eigenvalues separated by a distance ω (see Ref. [83]). The SFF also has an interpretation in terms of Poincaré recurrences; in fact, $K(t)$ is a lower bound to the number of Pauli strings \mathcal{P} that are mapped to themselves $U^{-t}\mathcal{P}U^t = \mathcal{P}$ after evolving for a time t . More precisely, it has been proven in Ref. [84] that

$$K(t) = 2^{-L} \sum_{\mathcal{P}} \langle \text{tr}[\mathcal{P}U^{-t}\mathcal{P}U^t] \rangle, \quad (11)$$

where the sum is over all Pauli strings \mathcal{P} . This identity holds for any unitary U , although only Clifford unitaries have the property that $U^{-t}\mathcal{P}U^t$ is equal or orthogonal to $\pm\mathcal{P}$. The possibility of this negative sign is responsible for the fact that Eq. (11) is not necessarily equal to the number of recurrences but is a lower bound.

The SFF has been studied extensively to explore the onset of random-matrix theory (RMT) behavior in the spectral properties of quantum systems [49,50,85–87]. In particular, it is proven in Ref. [83] that, for unitaries drawn from the uniform distribution (Haar measure) over $SU(2^L)$, the SFF reads

$$K(t) = \begin{cases} 2^{2L}, & \text{if } t = 0, \\ t, & \text{if } 1 \leq t \leq 2^L, \\ 2^L, & \text{if } t \geq 2^L. \end{cases} \quad (12)$$

Haar-distributed unitaries go also under the name of circular unitary ensemble (CUE). Equation (12) shows that the SFF increases as a linear ramp before reaching a plateau. Many-body chaotic systems are defined such that their SFFs increase linearly in time after an initial dip. The time at which the linear ramp starts is called the Thouless time, while the time at which the SFF reaches a plateau is called the Heisenberg time. A meaningful interpretation of these time scales requires rescaling, as discussed in, e.g., Refs. [35,88]. Figure 7 shows that the SFF of the periodic Clifford circuit that we are considering manifests an exponential ramp before reaching a plateau. A similar behavior is shown by quasifree fermions with chaotic single-particle dynamics [89,90]. (By quasifree fermions, we mean those having a Hamiltonian quadratic in the creation and annihilation operators.) The time in Fig. 7 is not rescaled and the value at which a plateau is reached is “evaluated” by inspection; therefore we call it plateau-time instead of Heisenberg time.

Building on the Clifford formalism, it is possible to compute Eq. (11) efficiently [84], without explicitly evaluating

the exponentially many terms. In order to do so, for any given Clifford unitary U , we define the group $H[U]$ of Pauli strings \mathcal{P} that are invariant under the action of the unitary U , namely $U^\dagger \mathcal{P} U = \pm \mathcal{P}$. Then, the method in Ref. [84] consists of finding a set of generators of the group $H[U]$, denoted $\text{gen}H[U]$, and exploiting the following identity:

$$|\text{tr}U|^2 = \begin{cases} 2^{|\text{gen}H[U]|}, & \text{if } U^\dagger \mathcal{P} U = +\mathcal{P}, \forall \mathcal{P} \in \text{gen}H[U], \\ 0, & \text{otherwise.} \end{cases}$$

Then, this is done for $U = U_{\text{per}}^t$, with U_{per} as defined in Eq. (1), and several values of t . Finally, one needs to average over many realizations of the circuit U_{per}^t . The exponential dependence of $K(t)$ on the number of generators already hints at the fact that the SFFs in Clifford circuits will exhibit strong fluctuations.

2. Numerical results

We now present our numerical results for the SFF in Floquet Clifford unitaries. Note that while the stabilizer formalism in principle allows for simulations of $U(t)$ with complexity scaling polynomially with L , the system sizes in the following are smaller than we are typically used to from other examples of Clifford numerics. The main reason for this is that computing $K(t)$ requires averaging over

a rather high number of circuit realizations, which makes simulations of larger L quite costly. Especially for 2D circuits, we find that extensive averaging is required to obtain converging results, since the calculation of $K(t)$ appears to be dominated by rare circuit realizations that yield very large values of $|\text{tr}U_{\text{per}}^t|^2$.

Figures 7(a) and 7(b) show $K(t)$ for 1D and 2D circuits with two different system sizes $L = 16, 24$. For the 1D circuit, we find that $K(t)$ exhibits a steep exponential increase at early times but quickly crosses over to a plateaulike behavior. The time at which this crossover takes place seems independent of L . Strikingly, however, this ‘‘plateau’’ is dominated by major fluctuations of the SFF. Note that (most of) these fluctuations are actual features of the dynamics of $K(t)$ and cannot be reduced further by circuit averaging. In fact, the data in Fig. 7 are already averaged over a substantial number (approximately 10^6) of random realizations. These fluctuations follow from the fact that the Clifford group has finite cardinality $|\mathcal{C}_L|$, which implies that the lengths t of the orbits (i.e., the smallest t such that $U^{-t} \mathcal{P} U^t = \mathcal{P}$) are divisors of $|\mathcal{C}_L|$. To see this, we recall Lagrange’s theorem: the order of a subgroup divides the order of the group. In particular, the smallest r such that $U^r = \mathbb{1}$ divides $|\mathcal{C}_L|$. Next, let us show that t is a divisor of r (and consequently a divisor of $|\mathcal{C}_L|$). If we assume the opposite, then $r = nt + m$ with $0 \leq m < t$, which implies that $\mathcal{P} = U^{-r} \mathcal{P} U^r = U^{-m} \mathcal{P} U^m$, which contradicts the fact that t is minimal.

Notably, the behavior of $K(t)$ changes in the case of 2D circuits [Fig. 7(b)]. Similarly to 1D, we again find an exponential increase of $K(t)$ at early times. However, in contrast to 1D, this ramp is cleaner and persists for a longer time in 2D. Specifically, comparing $K(t)$ for different L , we find that the end of the ramp occurs at $t_{\text{H}} \approx 2L$, which corresponds to the phase-space dimension of the Clifford dynamics (cf. Sec. IV A). For times $t > 2L$, the SFF displays strong fluctuations around the plateau value. We interpret this behavior of $K(t)$ as a signature of ergodic dynamics in phase space, analogous to quasifree fermions, as discussed above.

Let us explain why, in the 2D case, the plateau time grows with the system size as $t_{\text{H}} \approx 2L$, while in the 1D case t_{H} is independent of L . Equation (11) tells us that $K(t)$ reaches the plateau when evolving Pauli strings experience recurrences. In the 2D case, there is no localization; hence the evolution of Pauli strings is not restricted and can explore all the phase space. Recurrences reach a maximum at a time equal to the phase-space dimension $2L$ [analogously, in RMT, recurrences reach a maximum at a time equal to the Hilbert-space dimension given in Eq. (12)]. In the 1D case, the evolution of local Pauli operators is restricted to the localized regions, the size of which depends on U_{per} but not on the system size L . The evolution of nonlocal operators is also restricted because they can be decomposed into local operators with restricted dynamics.

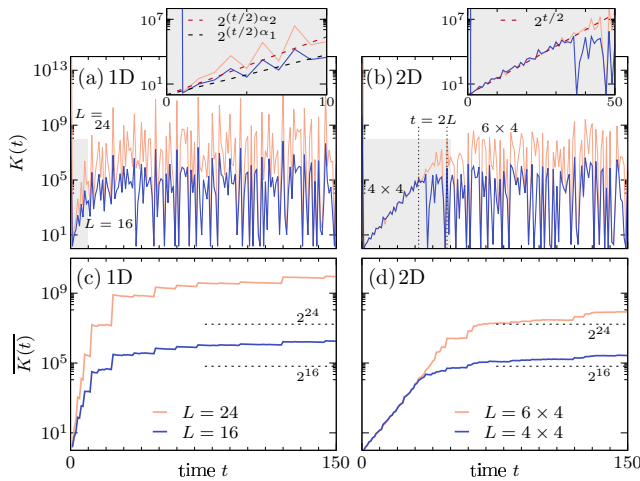


FIG. 7. The circuit-averaged $K(t)$ of Floquet Clifford unitaries for different system sizes L in (a) 1D and (b) 2D. The data are averaged over approximately 10^6 random-circuit realizations. The vertical dotted lines in (b) denote $t = 2L$, which approximately marks the end of the exponential ramp. The insets in (a) and (b) show the same data but now for shorter times [cf. the shaded areas in (a) and (b)]. In 2D, we find that the ramp is described by $K(t) \propto 2^{t/2}$, while in 1D $K(t) \propto 2^{(t/2)\alpha}$ with $\alpha \approx 2.5$ for $L = 16$ and $\alpha \approx 3.6$ for $L = 24$. In all cases, $K(t = 0) = 4^L$. (c),(d) The time-averaged SFF $\bar{K}(t)$ [Eq. 14] in (c) for 1D and in (d) for 2D. The horizontal dashed lines indicate the Hilbert-space dimension 2^L .

This follows from the fact that the evolution of a product of Pauli strings is equal to the product of the individual evolutions:

$$U^\dagger(t)[\mathcal{P}\mathcal{P}']U(t) = [U^\dagger(t)\mathcal{P}U(t)][U^\dagger(t)\mathcal{P}'U(t)]. \quad (13)$$

Now, let us discuss the long-time behavior of $K(t)$. In order to smooth the large fluctuations of $K(t)$, Figs. 7(c) and 7(d) show the time-averaged SFF

$$\overline{K(t)} = \frac{1}{t} \sum_{t'=0}^t K(t'). \quad (14)$$

The data of $\overline{K(t)}$ in Fig. 7(c) emphasize the fact that the initial ramp of $K(t)$ in 1D becomes steeper with increasing L . The large- t value of $\overline{K(t)}$ quantifies the degeneracies in U_{per} . This follows from

$$\begin{aligned} \overline{K(\infty)} &= \lim_{t \rightarrow \infty} \frac{1}{t} \sum_{t'=0}^t \left\langle \sum_{i,j=1}^{2^L} e^{i(E_i - E_j)t'} \right\rangle \\ &= \left\langle \sum_{i,j=1}^{2^L} \delta(E_i, E_j) \right\rangle \\ &= \left\langle \sum_E g_E^2 \right\rangle \geq 2^L, \end{aligned} \quad (15)$$

where E runs over all the quasienergies of U_{per} and g_E is the degeneracy of E (see Ref. [84]). Note that when $g_E = 1$ for all E , we have $\sum_E g_E^2 = 2^L$. In Fig. 7(c), we find that the long-time value of $\overline{K(t)}$ is notably higher than the Hilbert-space dimension 2^L , signaling the presence of degeneracy. In contrast, the RMT behavior of Eq. (12) implies that there are no degeneracies. An enhanced long-time value of $\overline{K(t)}$ can also be seen in 2D [see Fig. 7(d)], albeit less extreme in this case.

III. PROOF OF THEOREM 1

Let us consider the time evolution of a local operator acting on a single site at time $t = 0$. The support of this operator at later times ($t > 0$) is contained in the light cone represented in Fig. 3. However, in general, an operator may not have full support in the light cone (i.e., it acts as the identity in some events). In Sec. III A, we describe the boundary of the light cone with a directed graph and in Sec. III B, we describe the operator growth with a random directed graph.

Our goal is to lower bound the probability that the evolution of a local operator has support at the boundary at all times (i.e., nonidentity in at least one site of the boundary). A crucial observation to address this question is that the state of the operator at the boundary at time t depends

only on the state of the operator at the boundary at time $t - 1/2$ and does not depend on the state at the bulk of the light cone. Importantly, all unitary gates at the boundary at time t are statistically independent of the gates inside the light cone at previous times. This fact makes this problem mathematically tractable.

A. Directed-graph representation

The growth of the light-cone boundary can be represented by a directed graph G constructed in the following way. Each vertex of G represents a four-qubit unitary and each arrow represents a qubit that belongs to the boundary at a particular time t .

Construction of G

- (1) Add one vertex \bullet to represent the four-qubit unitary acting on the initial site at $t = 1/2$.
- (2) Add one outward-pointing arrow \nearrow for each of the qubits where the first unitary (potentially) propagates the signal at $t = 1/2$.
- (3) Repeat the following steps starting at $t = 1/2$:
 - (a) At the end of each outward-pointing arrow \nearrow at time t , add the vertex \bullet corresponding to the unitary acting at $t + 1/2$ on the qubit associated to the arrow \nearrow . (If two arrows represent qubits acted on by the same unitary at $t + 1/2$, then these two arrows point to the same vertex.)
 - (b) From each vertex \bullet corresponding to a unitary acting at $t + 1/2$, add one outward-pointing arrow for each of the qubits being acted on by the unitary \bullet and belonging to the boundary at $t + 1/2$.
- (4) Update $t \mapsto t + 1/2$ and repeat (a) and (b) up to infinity.

The construction of G , that is detailed in Figs. 3 and Fig. 8, shows G up to construction stage $t = 3/2$. Note that the infinite graph G has the following property: unitaries that act on the qubits that are on the corners of the (rectangular) boundary are represented by a vertex with one inward-pointing and three outward-pointing arrows. Similarly, unitaries that act on qubits on edges of the boundary have two inward-pointing and two outward-pointing arrows.

B. Random directed graph

In this section, we represent the random growth of an initially local operator evolving according to the random dynamics in Eq. (1) by a random directed graph G_{R} , defined below. This graph is constructed by allowing the arrows of G to be present or absent with certain probabilities. These probabilities are obtained from the statistical properties of the four-qubit gates $\mathcal{W}_{(x,y)}$. The property of light-speed operator growth up to time t happens when

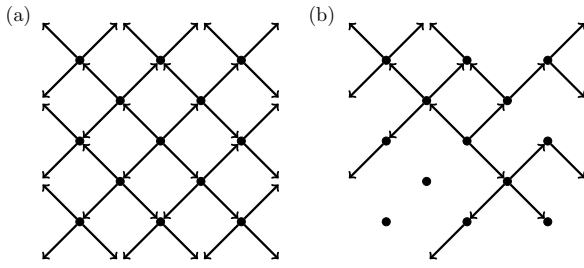


FIG. 8. The directed graph at $t = 3/2$. (a) the directed graph G . (b) An instance of the random directed graph G_R .

there is a path in G_R starting at the central vertex, following the directions of the arrows, and having length $2t$. In what follows, we bound the probability that G_R contains at least one such path.

There is, however, one minor point to consider. In principle, if a vertex in G_R has no inward-pointing arrows (i.e., the evolved operator has no support on the sites on which the gate associated to the vertex acts), then there should not be any outward-pointing arrows either. However, since we are considering directed paths from the origin, this is not a problem. That is to say, if there are no inward-pointing arrows to a vertex, the presence or absence of outward-pointing arrows is irrelevant, since a directed path from the origin cannot use this vertex anyway. Therefore, we consider the presence of outward-pointing arrows in a vertex of G_R to be statistically independent of the presence of inward-pointing arrows and independent of the presence of arrows in any other vertex. Still, the outward-pointing arrows of a particular vertex are not independent random variables. Each outward-pointing arrow i in a vertex has an associated random variable x_i , which takes the value $x_i = 1$ if the arrow is present and $x_i = 0$ if it is absent. The following lemma provides the joint probability distribution of the variables x_i .

Lemma 1.—For the vertex with four outward-pointing arrows x_1, x_2, x_3 , and x_4 , the probability of the presence of each arrow is

$$P(x_1, x_2, x_3, x_4) = \frac{1}{4^4 - 1} \begin{cases} 0, & \text{if } x_i = 0 \forall i, \\ 3^{\sum_i x_i}, & \text{otherwise,} \end{cases} \quad (16)$$

where $x_i = 1$ indicates that the i th arrow is present and $x_i = 0$ that it is absent. For the vertices with three outward-pointing arrows, the probability distribution is

$$P(x_1, x_2, x_3) = \frac{1}{4^4 - 1} \begin{cases} 3, & \text{if } x_i = 0 \forall i, \\ 4 \times 3^{\sum_i x_i}, & \text{otherwise.} \end{cases} \quad (17)$$

For the vertices with two outward-pointing arrows, the distribution is

$$P(x_1, x_2) = \frac{1}{4^4 - 1} \begin{cases} 4^2 - 1, & \text{if } x_1 = x_2 = 0, \\ 4^2 \times 3^{x_1 + x_2}, & \text{otherwise.} \end{cases} \quad (18)$$

Proof.—Let A be a four-qubit Pauli operator different than the identity and let W be a four-qubit random Clifford unitary. Let us consider the random four-qubit Pauli operator $WAW^\dagger = \lambda B = \lambda B_1 \otimes B_2 \otimes B_3 \otimes B_4$ and ignore the phase λ . Reference [14, Lemma 3] tells us that B is uniformly distributed over the $4^4 - 1$ combinations of $B_1, B_2, B_3, B_4 \in \{\mathbb{1}, \sigma_x, \sigma_y, \sigma_z\}$ different than $B_1 = B_2 = B_3 = B_4 = \mathbb{1}$. The factor 3^{x_i} follows from the fact that the value $x_i = 0$ denotes the one case $B_i = \mathbb{1}$, while the value $x_i = 1$ denotes the three cases $B_i \in \{\sigma_x, \sigma_y, \sigma_z\}$. This proves Eqs. (16), (17), and (18). ■

Definition 4.—The random directed graph G_R can be sampled by starting from G and, at each vertex, removing the outward-pointing arrows according to the probability distributions given in Eqs. (16), (17), and (18).

Definition 5.—An l -path in G_R is a sequence of l consecutive arrows starting at the central vertex and following the directions of the arrows (see Fig. 9).

In the lemma below, we show that in order to upper bound the probability that G_R has no l -path, it is enough to analyze its lower quadrant, as represented in Fig. 10.

Definition 6.—The directed graph G^Δ is the lower quadrant of G and the random directed graph G_R^Δ is the lower quadrant of G_R (see Fig. 10).

Lemma 2.—The probability that G_R has no l -path is upper bounded by the probability that G_R^Δ has no l -path, that is,

$$\text{prob}\{G_R \text{ has no } l\text{-path}\} \leq \text{prob}\{G_R^\Delta \text{ has no } l\text{-path}\}. \quad (19)$$

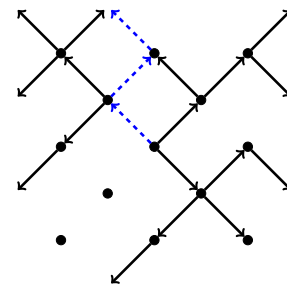


FIG. 9. This figure shows a 3-path in an instance of the random directed graph G_R .

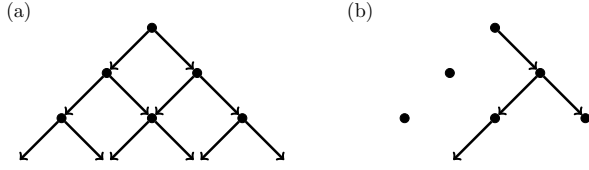


FIG. 10. (a) The graph G^Δ . (b) An instance of the random directed graph G_{IR}^Δ . Both are shown at time $t = 3/2$.

Proof.—By definition, if G_{R}^Δ has an l -path, then G_{R} has an l -path too; therefore, if G_{R} has no l -path, then G_{R}^Δ has no l -path. Using this, the bound follows. ■

C. Random graph with statistically independent arrows

In order to simplify the analysis, we define a new graph where the probability of the presence of each arrow is independent of the presence of other arrows. The next lemma shows that it is sufficient to analyze this new graph.

Definition 7.—The random directed graph G_{IR}^Δ is sampled by taking G^Δ and independently removing each arrow with probability

$$q := \text{prob}\{x = 0\} = \frac{1}{2} - \frac{1}{2}\sqrt{\frac{21}{85}} \gtrsim 0.25. \quad (20)$$

The subscript in G_{IR}^Δ denotes “independent random arrows.” The meaning of the value of q given above will become clear in the proof of Lemma 3. As mentioned above, we have the following.

Lemma 3.—The probability that G_{R}^Δ has no l -path is upper bounded by the probability that G_{IR}^Δ has no l -path:

$$\text{prob}\{G_{\text{R}}^\Delta \text{ has no } l\text{-path}\} \leq \text{prob}\{G_{\text{IR}}^\Delta \text{ has no } l\text{-path}\}. \quad (21)$$

Proof.—First, note that the probability distribution of outward-pointing arrows from different vertices are independent and hence we focus only on a single vertex with two outward-pointing arrows. Second, we construct a matrix with the probability distribution $P(x_1, x_2)$ for the presence of outward-pointing arrows [see Eq. (18)] as

$$\begin{pmatrix} P(0,0) & P(0,1) \\ P(1,0) & P(1,1) \end{pmatrix} = \frac{1}{255} \begin{pmatrix} 15 & 16 \times 3 \\ 16 \times 3 & 16 \times 9 \end{pmatrix}. \quad (22)$$

Third, we increase $\text{prob}\{x_1 = x_2 = 0\} \rightarrow P(0,0) + \epsilon$ and decrease $\text{prob}\{x_1 = x_2 = 1\} \rightarrow P(1,1) - \epsilon$ until the

distribution becomes of product form

$$\begin{aligned} \begin{pmatrix} P(0,0) + \epsilon & P(0,1) \\ P(1,0) & P(1,1) - \epsilon \end{pmatrix} &= \begin{pmatrix} \frac{1}{17} + \epsilon & \frac{16}{85} \\ \frac{16}{85} & \frac{48}{85} - \epsilon \end{pmatrix} \quad (23) \\ &= \begin{pmatrix} q^2 & q(1-q) \\ q(1-q) & (1-q)^2 \end{pmatrix}. \quad (24) \end{aligned}$$

We want to find the minimum $\epsilon > 0$ such that there is $q \in [0, 1]$ satisfying the above equality. Clearly, this transformation cannot increase the likelihood of an l -path. The above matrix is of product form when its determinant is zero, in fact the second column of the last matrix in Eq. (23) is obtained from the first one by multiplying by $(1-q)/q$:

$$\det \begin{pmatrix} \frac{1}{17} + \epsilon & \frac{16}{85} \\ \frac{16}{85} & \frac{48}{85} - \epsilon \end{pmatrix} = 0. \quad (25)$$

This equation has smallest positive solution $\epsilon = 1/170$ ($43 - \sqrt{1785}$) ≈ 0.0044 , which implies that

$$q = \frac{1}{17} + \epsilon + \frac{16}{85} = \frac{1}{2} - \frac{1}{2}\sqrt{\frac{21}{85}}. \quad (26)$$

This proves the statement of the lemma. ■

D. Dual graph

Definition 8.—The graph $G_{\text{IR}}^{\Delta*}$ dual to G_{IR}^Δ has vertices located at the faces of G_{IR}^Δ . The presence of a (nondirected) edge in $G_{\text{IR}}^{\Delta*}$ corresponds to the absence of the arrow that it intersects in G_{IR}^Δ . Therefore, the probability q^* that an edge is absent in $G_{\text{IR}}^{\Delta*}$ is equal to the probability that an arrow is present in G_{IR}^Δ , that is, $q^* = 1 - q$, where q is defined in Eq. (20). Figure 11 displays the graph dual to that of Fig. 10.

Definition 9.—A d -wall is a set of d consecutive edges that connect the left side of $G_{\text{IR}}^{\Delta*}$ to the right side.

Lemma 4.—If $G_{\text{IR}}^{\Delta*}$ contains a d -wall, then G_{IR}^Δ contains no l -path of length $l \geq d$.

Proof.—This follows from the fact that a d -wall must start in one of the first d vertices of the left and that l -paths always go downward. ■

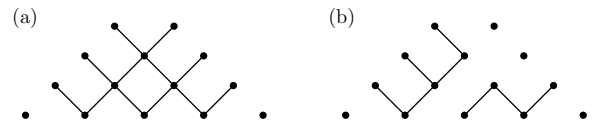


FIG. 11. The dual graph. (a) The dual graph $G^{\Delta*}$. (b) the instance of the random graph $G_{\text{IR}}^{\Delta*}$ that is dual to the instance of G_{IR}^Δ shown in Fig. 10.

Lemma 5.—The probability that $G_{\text{IR}}^{\Delta*}$ has a d -wall for some d satisfies

$$\text{prob}\{\exists d : G_{\text{IR}}^{\Delta*} \text{ has } d\text{-wall}\} \leq 0.56. \quad (27)$$

Proof.—Let us start by upper bounding the maximal number of d -walls N_d that $G_{\text{IR}}^{\Delta*}$ can have. Consider a d -wall starting at a specific vertex position on the left side of $G_{\text{IR}}^{\Delta*}$. For the choice of the first edge in the path there is only one possibility, for the choice of each of the following $d - 2$ edges there are at most three possibilities, and for the final edge there is a single choice (again). Hence, we can upper bound the number of d -walls starting at a specific vertex on the left side by 3^{d-2} . It is worth noting that this upper bound includes many paths that do not connect the left and right sides and, hence, do not actually form a d -wall. The total number of vertices that can be the initial vertex (left side) of a d -wall is $d - 1$. Hence, we have $N_d \leq (d - 1)3^{d-2}$. In order to obtain a better bound, we note that when the starting vertex of a d -wall is either the first or $(d - 1)$ th from the top, then there is only one possible choice of d -wall. Therefore, we obtain

$$N_d \leq (d - 3)3^{d-2} + 2. \quad (28)$$

Direct counting gives the exact number of d -walls for small values of d , which is displayed in the following table:

d	2	3	4	5	6
N_d	1	2	3	6	18

(29)

Next, the probability that $G_{\text{IR}}^{\Delta*}$ contains a particular d -wall in $G^{\Delta*}$ is $(1 - q^*)^d = q^d$. Therefore, the probability that $G_{\text{IR}}^{\Delta*}$ has at least one d -wall satisfies

$$\text{prob}\{G_{\text{IR}}^{\Delta*} \text{ has } d\text{-wall}\} \leq N_d q^d. \quad (30)$$

Finally, the probability that $G_{\text{IR}}^{\Delta*}$ contains a d -wall of any length d satisfies

$$\begin{aligned} & \text{prob}\{\exists d : G_{\text{IR}}^{\Delta*} \text{ has } d\text{-wall}\} \\ & \leq \sum_{d=2}^{\infty} \text{prob}\{G_{\text{IR}}^{\Delta*} \text{ has } d\text{-wall}\} \leq \sum_{d=2}^{\infty} N_d q^d \end{aligned} \quad (31)$$

$$\leq \sum_{d=2}^6 N_d q^d + \sum_{d=7}^{\infty} [(d - 3)3^{d-2} + 2] q^d \quad (32)$$

$$\approx 0.56, \quad (33)$$

where we use the table in Eq. (29) and the bound in Eq. (28). ■

Combining Lemmas 2, 3, 4, and 5 we can prove our main result.

Remark.—What follows is an equivalent statement of Theorem 1 that has appeared previously in the paper.

Theorem 1.—The probability that G_{R} has an l -path of infinite length $l = \infty$ satisfies

$$\text{prob}\{G_{\text{R}} \text{ has } \infty\text{-path}\} \geq 0.44. \quad (34)$$

To conclude this section, let us note that while this proof of Theorem 1 establishes the absence of localization in the 2D Floquet Clifford circuits given in Eq. (1), the lower bound given in Eq. (34) is probably not tight for practical purposes. Specifically, in our simulations of 2D circuits of *finite size* $L < \infty$, we find nontrivial operator support on the light-cone boundary for virtually all times and all random-circuit realizations, such as in the example depicted in Fig. 1(b).

IV. COMPARING CLIFFORD DYNAMICS WITH QUASIFREE BOSONS AND FERMIONS

In this section, we argue that Clifford dynamics shares features with quasifree systems, along with certain similarities with chaotic systems. Therefore, in order to elucidate the full landscape of quantum many-body phenomena, it is important to understand the properties of Clifford systems.

A. General dynamics

Similarly to quasifree fermions, Clifford unitaries can be represented by symplectic matrices in a phase space of dimension exponentially smaller than the Hilbert space. This dimensional reduction allows for efficient simulation of the evolution of any local or Pauli operator with a classical computer [64]. The efficient simulability of Clifford circuits can also be understood with respect to the non-negativity of the associated Wigner function in phase space [91,92]. In particular, this non-negativity of the Wigner function of stabilizer states is analogous to the non-negative Wigner function of the Gaussian states corresponding to models with a quadratic Hamiltonian [93,94]. Furthermore, we see in Sec. III that Clifford dynamics allow for a certain degree of analytical tractability, similarly to other types of integrable models.

Unlike quasifree systems, the Clifford phase space is a vector space over a finite field (\mathbb{Z}_2^{2N} is the phase space of N qubits); hence evolution cannot be continuous in time. That is, we can have Floquet-type but not Hamiltonian-type dynamics. For the same reason, the evolution operator cannot be diagonalized into noninteracting “modes.” Related to this is the fact that some aspects of typical Clifford dynamics cannot be understood in terms of free or weakly interacting particles [see, e.g., the dynamics in Fig. 1(a)].

Uniformly distributed (i.e., Haar) unitaries are resembled much more from random Clifford unitaries than from

random quasifree unitaries. This can be made quantitative by using the notion of unitary design [95]. On the one hand, random quasifree unitaries cannot even generate a 1-design, because their evolution operators commute with the number operator (bosons) or the parity operator (fermions). On the other hand, random Clifford unitaries generate a 3-design [66,67] and almost a 4-design [96].

As discussed in Sec. IID, the SFF of Clifford unitaries corresponds to that of quasifree fermions with chaotic single-particle dynamics, as in the quadratic Sachdev-Ye-Kitaev (SYK) model [89,90].

B. Translation-invariant local dynamics

In Ref. [97], the authors analyze a translation-invariant Clifford Floquet model in one spatial dimension. They prove that the system has no local or quasilocal integrals of motion. More specifically, any operator that commutes with the evolution operator acts on an extensive number of sites with couplings among them that do not decay with the distance. This is very different to what happens with quasifree systems, which have an extensive number of local conservation laws (see Refs. [98,99]).

Unlike quasifree systems, the Clifford model analyzed in Ref. [97] enjoys a strong form of eigenstate thermalization. That is, all eigenstates are maximally entangled in the sense that the reduced density matrix of any connected region is equal to the maximally mixed state (in the thermodynamic limit). In other words, none of the eigenstates satisfy an entanglement area law.

C. Disordered local dynamics

The 1D analog of our model (analyzed in detail in Ref. [14]) displays a strong form of localization produced by the emergence of left- and right-blocking walls at random locations [see Fig. 1(a)]. Until now, this strong form of localization, reminiscent of Anderson localization, has only been found in systems of free or weakly interacting particles. In strongly interacting systems, the localization is in some sense weaker (many-body localization), since the width of the light cones grows as the logarithm of time. The Clifford dynamics appear to be some form of hybrid, as they cannot be understood entirely in terms of free or weakly interacting particles but yet they display Anderson-type localization in 1D. Remarkably, however, the similarity in their localization properties does not carry over to 2D. More specifically, while we show in this paper that localization is absent in 2D random Floquet Clifford circuits, quasifree systems, such as noninteracting fermions, are well known to localize in 2D lattices even in the presence of arbitrarily weak disorder [100].

V. CONCLUSIONS

We introduce a Floquet model comprised of random Clifford gates and prove as a main result that it does

not localize in two spatial dimensions, despite having strong disorder. More precisely, we prove the existence of operators that grow ballistically and we see numerically that this holds for almost all operators. This result is notable because, as discussed in Sec. IV, this model shares certain features of other integrable models and 2D integrable systems with strong disorder are usually expected to localize, e.g., noninteracting lattice fermions in a random potential, as originally considered in the case of Anderson localization. We substantiate our analytical findings by numerically demonstrating the absence (presence) of localization in 2D (1D) Floquet Clifford circuits. Furthermore, we study the SFF of the Floquet unitary, which is a key quantity in the context of quantum chaos. To the best of our knowledge, our work is the first to study the SFF in 2D Clifford circuits, complementing the analysis of Ref. [84], which has focused on 1D. We unveil that the SFF behaves in a drastically different way in 2D. In particular, we observe a clean exponential ramp persisting up to a time that scales linearly with the system size, which we interpret as a signature of ergodic dynamics in phase space.

It is worth noting that, since the definition of light-speed growth only concerns the boundary of the light cone, our results also apply to the time-dependent (non-Floquet) version of the model, where new gates are randomly generated at each time step. For the same reason, our results for the 2D model extend to time-periodic circuits with time period larger than 2. The difference between models with period equal to 2 and models with a larger period or time-dependent models could manifest itself in the interior of the light cone. While the time-dependent model has completely ergodic dynamics, Fig. 5(c) suggests that our time-periodic model is not far from it. While, with our analytical methods, we cannot address the interior of the light cone, it might be interesting to extend our numerical analysis to probe whether the bulk of the light cone is indeed featureless or whether the Floquet circuit induces some structure on the Pauli strings that are sampled during the dynamics. Such potential differences compared with fully ergodic dynamics may be reflected in, e.g., the behavior of higher-order and nonlocal correlation functions that go beyond the local probe considered in Fig. 5.

In future work, we would like to study the case where instead of sampling gates from the Clifford group, we sample from the full unitary group $SU(4)$. In the case of time-dependent circuits, this has been well studied in, e.g., Refs. [3,6,101], whereas the case of time-periodic quantum circuits in one spatial dimension has been studied in, e.g., Refs. [49–51]. In this context, one promising approach to interpolate between Clifford dynamics and more generic Haar-random circuits is to consider circuits composed mainly of Clifford elements interspersed with a (low) density of non-Clifford gates, the latter acting as a seed of chaos that may enhance the ergodic aspects of

the dynamics further [102,103], despite the loss of classical simulability [104]. Such a procedure may also help us to better understand the apparent differences as well as similarities of Clifford dynamics and other notions of integrability [89,90], a detailed exploration of which we believe to be an important direction of future work.

The localization proven for the dynamics of a period-2 1D QCA of Cliffords in Ref. [14] and corroborated numerically in Fig. 5, as seen above, is known to disappear for a time-dependent circuit, that corresponds to a periodic circuit of infinite period, as also follows from Ref. [14]. Numerical investigations performed in Ref. [105] show that the 1D circuit with period equal to 4 still localizes with the appearance of hard walls that nevertheless are characterized by a larger localization length than the period-2 case.

Finally, we would like to comment on the connections between our methods and directed-percolation theory [106,107]. Both cases analyze the presence of infinitely long paths that start at the origin in random directed graphs. However, in our case, and in that of general cellular automata, the arrows that emerge from the same vertex are not statistically independent (see Lemma 1), while in the standard theory of directed percolation they are.

In conclusion, our work provides a new perspective on the possibility of using Clifford circuits to simulate certain novel nonequilibrium quantum phenomena. We expect that our work will inform future studies that aim to use Clifford circuits as starting points to understand more generic quantum dynamics.

The rigorous understanding of localization and chaos in this solvable limit provides a basis for toy models to simulate nonequilibrium states in kinetically constrained models. The classical simulability of Clifford circuits can play a constructive role for benchmarking the performance of noisy intermediate-scale quantum computers for quantum simulation and distinguishing between classical and quantum effects in them.

ACKNOWLEDGMENTS

T.F. acknowledges financial support by the Engineering and Physical Sciences Research Council (Grants No. EP/L015242/1 and No. EP/S005021/1) and is grateful to the Heilbronn Institute for Mathematical Research for support. L.M. and D.T. acknowledge financial support by the UK's Engineering and Physical Sciences Research Council (Grant No. EP/R012393/1). D.T. also acknowledges support from UK Research and Innovation Grant No. EP/R029075/1. J.R. and A.P. acknowledge funding by the European Research Council (ERC) under the European Union Horizon 2020 research and innovation program (Grant Agreement No. 853368). J.R. also received funding from the European Union's Horizon Europe programme under the Marie Skłodowska-Curie grant agreement No.

101060162, and the Packard Foundation through a Packard Fellowship in Science and Engineering.

APPENDIX: LOCALIZATION LENGTH IN THE 1D MODEL

We present here a result that builds upon, and improves, Ref. [14, Theorem 25]. Let us first informally restate this theorem. The periodic dynamics of a 1D QCA of two-qubit gates of uniformly sampled Clifford unitaries, represented as the inbox of Fig. 1, and in Ref. [14, Fig. 1], are such that the probability of appearance of a right- (or left-) blocking wall is at least 0.12. If we consider only walls with a penetration length equal to 1, meaning that if, e.g., a right-blocking wall is placed at $x = 0$, then the support of an operator hitting that wall is allowed to flow only up to $x = 1$, and then the probability of the appearance of a wall is exactly equal to 0.12. The proof of this statement rests on the use of the phase-space formalism for Clifford unitaries. The following corollary gives an upper bound on the average spread of the support of an operator that is initially nonidentity only at one point. This spread is the localization length μ that is given in Definition 1.

Corollary 1.—The periodic dynamics of a 1D QCA of two-qubit gates of uniformly sampled Clifford unitaries are such that given an operator initially supported only on site $x = 0$, the probability that a wall blocking its dynamics appears at a distance l and that no other wall appears at $\{0, \dots, l - 1\}$, is $ce^{-l/\mu}$, with $c \approx 0.07$ and μ upper bounded by 13.2.

Proof.—Let us assume, for simplicity, that we consider a wall blocking propagation toward the right. According to the phase-space formalism, as detailed in Ref. [14, see esp. Secs. II E and VII], the absences of walls at neighboring positions, e.g., $x = 0$ and $x = 1$, are correlated events. In fact, they satisfy the conditions $C_1 C_0 \neq 0$ and/or $C_1 D_0 A_1 C_0 \neq 0$ for the absence of a wall at $x = 0$ and $C_2 C_1 \neq 0$ and/or $C_2 D_1 A_2 C_1 \neq 0$ for the absence of a wall at $x = 1$. Denoting by W_l the presence of a wall at $x = l$ and by \bar{W}_l the absence of a wall at $x = l$, we see that $\text{Prob}(\bar{W}_1 \wedge \bar{W}_0) = \text{Prob}(\bar{W}_1 | \bar{W}_0) \text{Prob}(\bar{W}_0)$. This leads to a Markov chain; in fact, the absence of a wall at $x = 2$ involves the matrix blocks $\{C_3, D_2, A_3, C_2\}$ and we see that none of them appears in the condition defining \bar{W}_0 . This means that the probability of having a wall at $x = l$ and no other wall at $\{0, \dots, l - 1\}$ is given by

$$\begin{aligned} \text{Prob}(W_l \wedge \bar{W}_{l-1} \wedge \dots \wedge \bar{W}_0) &= \\ &= \text{Prob}(W_l | \bar{W}_{l-1}) \text{Prob}(\bar{W}_1 | \bar{W}_0)^{l-1} \text{Prob}(\bar{W}_0) \\ &= (1 - \text{Prob}(\bar{W}_l | \bar{W}_{l-1})) \text{Prob}(\bar{W}_1 | \bar{W}_0)^{l-1} \text{Prob}(\bar{W}_0) \end{aligned}$$

$$\begin{aligned}
 &= (1 - \text{Prob}(\overline{W}_1|\overline{W}_0)) \text{Prob}(\overline{W}_1|\overline{W}_0)^{l-1} \text{Prob}(\overline{W}_0) \\
 &= \frac{(1 - \text{Prob}(\overline{W}_1|\overline{W}_0)) \text{Prob}(\overline{W}_0)}{\text{Prob}(\overline{W}_1|\overline{W}_0)} \text{Prob}(\overline{W}_1|\overline{W}_0)^l.
 \end{aligned} \tag{A1}$$

With the aid of computer software, we exactly evaluate $\text{Prob}(\overline{W}_1|\overline{W}_0) = 0.927$ and we recall from Ref. [14] that $\text{Prob}(\overline{W}_0) = 0.88$. Then, Eq. (A1) implies that

$$\text{Prob}(W_l \wedge \overline{W}_{l-1} \wedge \dots \wedge \overline{W}_0) = ce^{-\frac{l}{\mu}}, \tag{A2}$$

with

$$c = \frac{(1 - \text{Prob}(\overline{W}_1|\overline{W}_0)) \text{Prob}(\overline{W}_0)}{\text{Prob}(\overline{W}_1|\overline{W}_0)} \approx 0.07 \tag{A3}$$

$$\mu = -\frac{1}{\log(\text{Prob}(\overline{W}_1|\overline{W}_0))} \approx 13.2. \tag{A4}$$

This proof takes into account walls with penetration length equal to 1, described by Ref. [14, Figs. 4 and 5]. Walls with a larger penetration length are also allowed by the dynamics: taking them into account would lead to a shorter localization length, as confirmed by the numerics that lead to Fig. 5 and therefore the value $\mu \approx 13.2$ is an upper bound. ■

We comment about normalization of probability as a check that Corollary 1 is consistent. In the limit of an infinite system, the probability of having no wall at all is vanishing. This follows from the proof of Corollary 1, where instead of evaluating $\text{Prob}(W_l \wedge \overline{W}_{l-1} \wedge \dots \wedge \overline{W}_0)$, we consider $\text{Prob}(\overline{W}_l \wedge \overline{W}_{l-1} \wedge \dots \wedge \overline{W}_0)$. This means that the probability of having at least one wall equals 1. The probability of having at least one wall is the sum of the probability of having a wall in $x = 0$ and whatever else (namely a configuration of gates that might or might not give rise to a wall), plus the probability of having no wall in $x = 0$ and a wall in $x = 1$ and whatever else, plus the probability of having no wall in $x = 0$ and no wall in $x = 1$ and a wall in $x = 2$ and whatever else, and so on. This means that

$$1 = \text{Prob}(W_0) + \sum_{l=1}^{\infty} \text{Prob}(W_l \wedge \overline{W}_{l-1} \wedge \dots \wedge \overline{W}_0). \tag{A5}$$

It is possible to verify that Eq. (A5) is implied by Eqs. (A2), (A3), and (A4). We then have the normalized probability distribution $P(l)$ for the appearance of a wall at

$x = l$ and no prior wall:

$$P(l) = \begin{cases} \text{Prob}(W_0) = 0.12, & \text{with } l = 0, \\ ce^{-\frac{l}{\mu}}, & \text{with } l \geq 1. \end{cases} \tag{A6}$$

This implies that the average position of a wall is given by

$$\langle l \rangle = \sum_{l=1}^{\infty} lce^{-\frac{l}{\mu}} = \text{Prob}(\overline{W}_0) \mu + \mathcal{O}((1 - \text{Prob}(\overline{W}_1|\overline{W}_0))^2). \tag{A7}$$

This gives the relationship between the average position of a wall and the localization length μ in the limit of a large system.

-
- [1] A. Polkovnikov, K. Sengupta, A. Silva, and M. Vengalattore, Colloquium: Nonequilibrium dynamics of closed interacting quantum systems, *Rev. Mod. Phys.* **83**, 863 (2011).
 - [2] A. Nahum, J. Ruhman, S. Vijay, and J. Haah, Quantum Entanglement Growth under Random Unitary Dynamics, *Phys. Rev. X* **7**, 031016 (2017).
 - [3] A. Nahum, S. Vijay, and J. Haah, Operator Spreading in Random Unitary Circuits, *Phys. Rev. X* **8**, 021014 (2018).
 - [4] C. von Keyserlingk, T. Rakovszky, F. Pollmann, and S. Sondhi, Operator Hydrodynamics, OTOCs, and Entanglement Growth in Systems without Conservation Laws, *Phys. Rev. X* **8**, 021013 (2018).
 - [5] T. Rakovszky, F. Pollmann, and C. von Keyserlingk, Diffusive Hydrodynamics of Out-of-Time-Ordered Correlators with Charge Conservation, *Phys. Rev. X* **8**, 031058 (2018).
 - [6] V. Khemani, A. Vishwanath, and D. A. Huse, Operator Spreading and the Emergence of Dissipative Hydrodynamics under Unitary Evolution with Conservation Laws, *Phys. Rev. X* **8**, 031057 (2018).
 - [7] T. Zhou and A. Nahum, Emergent statistical mechanics of entanglement in random unitary circuits, *Phys. Rev. B* **99**, 174205 (2019).
 - [8] F. G. Brandão, W. Chemissany, N. Hunter-Jones, R. Kueng, and J. Preskill, Models of Quantum Complexity Growth, *PRX Quantum* **2**, 030316 (2021).
 - [9] A. C. Potter and R. Vasseur, in *Entanglement in Spin Chains: From Theory to Quantum Technology Applications*, edited by A. Bayat, S. Bose, and H. Johannesson (Springer International Publishing, Cham, 2022), p. 211 (specific prepublication chapter <https://arxiv.org/abs/2111.08018>).
 - [10] S. Moudgalya, A. Prem, D. A. Huse, and A. Chan, Spectral statistics in constrained many-body quantum chaotic systems, *Phys. Rev. Res.* **3**, 023176 (2021).
 - [11] S. Gopalakrishnan and B. Zakerov, Facilitated quantum cellular automata as simple models with non-thermal eigenstates and dynamics, *Quantum Sci. Technol.* **3**, 044004 (2018).

- [12] B. Bertini, P. Kos, and T. Prosen, Exact Correlation Functions for Dual-Unitary Lattice Models Dimensions, *Phys. Rev. Lett.* **123**, 210601 (2019).
- [13] P. W. Claeys and A. Lamacraft, Ergodic and Nonergodic Dual-Unitary Quantum Circuits with Arbitrary Local Hilbert Space Dimension, *Phys. Rev. Lett.* **126**, 100603 (2021).
- [14] T. Farshi, D. Toniolo, C. E. González-Guillén, Á. M. Alhambra, and L. Masanes, Mixing and localization in random time-periodic quantum circuits of Clifford unitaries, *J. Math. Phys.* **63**, 032201 (2022).
- [15] J. Richter, O. Lunt, and A. Pal, Transport and entanglement growth in long-range random Clifford circuits, *Phys. Rev. Res.* **5**, L012031 (2023).
- [16] F. Arute *et al.*, Quantum supremacy using a programmable superconducting processor, *Nature* **574**, 505 (2019).
- [17] X. Mi *et al.*, Information scrambling in quantum circuits, *Science* **374**, 1479 (2021).
- [18] L. D'Alessio, Y. Kafri, A. Polkovnikov, and M. Rigol, From quantum chaos and eigenstate thermalization to statistical mechanics and thermodynamics, *Adv. Phys.* **65**, 239 (2016).
- [19] C. Gogolin and J. Eisert, Equilibration, thermalisation, and the emergence of statistical mechanics in closed quantum systems, *Rep. Prog. Phys.* **79**, 056001 (2016).
- [20] L. Vidmar and M. Rigol, Generalized Gibbs ensemble in integrable lattice models, *J. Stat. Mech: Theory Exp.* **2016**, 064007 (2016).
- [21] R. Nandkishore and D. A. Huse, Many-body localization and thermalization in quantum statistical mechanics, *Annu. Rev. Condens. Matter Phys.* **6**, 15 (2015).
- [22] D. A. Abanin, E. Altman, I. Bloch, and M. Serbyn, Colloquium: Many-body localization, thermalization, and entanglement, *Rev. Mod. Phys.* **91**, 021001 (2019).
- [23] G. Stolz, An introduction to the mathematics of anderson localization, *Contemp. Math.* **552**, 71 (2011).
- [24] M. Aizenman and S. Warzel, *Random Operators: Disorder Effects on Quantum Spectra and Dynamics* (American Mathematical Society, 2015).
- [25] P. W. Anderson, Absence of diffusion in certain random lattices, *Phys. Rev.* **109**, 1492 (1958).
- [26] E. Hamza, R. Sims, and G. Stolz, Dynamical localization in disordered quantum spin systems, *Commun. Math. Phys.* **315**, 215 (2012).
- [27] H. Abdul-Rahman, B. Nachtergaele, R. Sims, and G. Stolz, Entanglement dynamics of disordered quantum XY chains, *Lett. Math. Phys.* **106**, 649 (2016).
- [28] D.-L. Deng, X. Li, J. H. Pixley, Y.-L. Wu, and S. Das Sarma, Logarithmic entanglement lightcone in many-body localized systems, *Phys. Rev. B* **95**, 024202 (2017).
- [29] M. Žnidarič, T. Prosen, and P. Prelovšek, Many-body localization in the Heisenberg xxz magnet in a random field, *Phys. Rev. B* **77**, 064426 (2008).
- [30] J. H. Bardarson, F. Pollmann, and J. E. Moore, Unbounded Growth of Entanglement in Models of Many-Body Localization, *Phys. Rev. Lett.* **109**, 017202 (2012).
- [31] M. Serbyn, Z. Papić, and D. A. Abanin, Universal Slow Growth of Entanglement in Interacting Strongly Disordered Systems, *Phys. Rev. Lett.* **110**, 260601 (2013).
- [32] J. Z. Imbrie, On many-body localization for quantum spin chains, *J. Stat. Phys.* **163**, 998 (2016).
- [33] W. De Roeck and F. Huveneers, Stability and instability towards delocalization in many-body localization systems, *Phys. Rev. B* **95**, 155129 (2017).
- [34] J. Šuntajs, J. Bonča, T. Prosen, and L. Vidmar, Ergodicity breaking transition in finite disordered spin chains, *Phys. Rev. B* **102**, 064207 (2020).
- [35] J. Šuntajs, J. Bonča, T. Prosen, and L. Vidmar, Quantum chaos challenges many-body localization, *Phys. Rev. E* **102**, 062144 (2020).
- [36] P. Sierant, M. Lewenstein, and J. Zakrzewski, Polynomially Filtered Exact Diagonalization Approach to Many-Body Localization, *Phys. Rev. Lett.* **125**, 156601 (2020).
- [37] A. Morningstar, L. Colmenarez, V. Khemani, D. J. Luitz, and D. A. Huse, Avalanches and many-body resonances in many-body localized systems, *Phys. Rev. B* **105**, 174205 (2022).
- [38] W. De Roeck and J. Z. Imbrie, Many-body localization: Stability and instability, *Philos. Trans. R. Soc. A: Math., Phys. Eng. Sci.* **375**, 20160422 (2017).
- [39] T. B. Wahl, A. Pal, and S. H. Simon, Signatures of the many-body localized regime in two dimensions, *Nat. Phys.* **15**, 164 (2018).
- [40] D. Sels and A. Polkovnikov, Dynamical obstruction to localization in a disordered spin chain, *Phys. Rev. E* **104**, 054105 (2021).
- [41] M. Kiefer-Emmanouilidis, R. Unanyan, M. Fleischhauer, and J. Sirker, Evidence for Unbounded Growth of the Number Entropy in Many-Body Localized Phases, *Phys. Rev. Lett.* **124**, 243601 (2020).
- [42] R. Ghosh and M. Žnidarič, Resonance-induced growth of number entropy in strongly disordered systems, *Phys. Rev. B* **105**, 144203 (2022).
- [43] J. Richter and A. Pal, Many-body localization and delocalization dynamics in the thermodynamic limit, *Phys. Rev. B* **105**, 1220405 (2022).
- [44] L. D'Alessio and M. Rigol, Long-Time Behavior of Isolated Periodically Driven Interacting Lattice Systems, *Phys. Rev. X* **4**, 041048 (2014).
- [45] A. Lazarides, A. Das, and R. Moessner, Equilibrium states of generic quantum systems subject to periodic driving, *Phys. Rev. E* **90**, 012110 (2014).
- [46] C. Sünderhauf, D. Pérez-García, D. A. Huse, N. Schuch, and J. I. Cirac, Localization with random time-periodic quantum circuits, *Phys. Rev. B* **98**, 134204 (2018).
- [47] V. Khemani, M. Hermele, and R. Nandkishore, Localization from Hilbert space shattering: From theory to physical realizations, *Phys. Rev. B* **101**, 174204 (2020).
- [48] S. Pai, M. Pretko, and R. M. Nandkishore, Localization in Fractonic Random Circuits, *Phys. Rev. X* **9**, 021003 (2019).
- [49] P. Kos, M. Ljubotina, and T. Prosen, Many-Body Quantum Chaos: Analytic Connection to Random Matrix Theory, *Phys. Rev. X* **8**, 021062 (2018).
- [50] B. Bertini, P. Kos, and T. Prosen, Exact Spectral Form Factor in a Minimal Model of Many-Body Quantum Chaos, *Phys. Rev. Lett.* **121**, 264101 (2018).

- [51] B. Bertini, P. Kos, and T. Prosen, Operator entanglement in local quantum circuits I: Chaotic dual-unitary circuits, *SciPost Phys.* **8**, 67 (2020).
- [52] A. Chan, A. De Luca, and J. T. Chalker, Spectral Statistics in Spatially Extended Chaotic Quantum Many-Body Systems, *Phys. Rev. Lett.* **121**, 060601 (2018).
- [53] A. Chan, A. De Luca, and J. T. Chalker, Solution of a Minimal Model for Many-Body Quantum Chaos, *Phys. Rev. X* **8**, 041019 (2018).
- [54] M. Bukov, L. D'Alessio, and A. Polkovnikov, Universal high-frequency behavior of periodically driven systems: From dynamical stabilization to Floquet engineering, *Adv Phys.* **64**, 139 (2015).
- [55] V. Khemani, A. Lazarides, R. Moessner, and S. Sondhi, Phase Structure of Driven Quantum Systems, *Phys. Rev. Lett.* **116**, 250401 (2016).
- [56] D. V. Else, B. Bauer, and C. Nayak, Floquet Time Crystals, *Phys. Rev. Lett.* **117**, 090402 (2016).
- [57] E. Knill, D. Leibfried, R. Reichle, J. Britton, R. B. Blakestad, J. D. Jost, C. Langer, R. Ozeri, S. Seidelin, and D. J. Wineland, Randomized benchmarking of quantum gates, *Phys. Rev. A* **77**, 012307 (2008).
- [58] E. Magesan, J. M. Gambetta, and J. Emerson, Scalable and Robust Randomized Benchmarking of Quantum Processes, *Phys. Rev. Lett.* **106**, 180504 (2011).
- [59] E. Onorati, A. H. Werner, and J. Eisert, Randomized Benchmarking for Individual Quantum Gates, *Phys. Rev. Lett.* **123**, 060501 (2019).
- [60] Y. Li, X. Chen, and M. P. A. Fisher, Quantum Zeno effect and the many-body entanglement transition, *Phys. Rev. B* **98**, 205136 (2018).
- [61] Y. Li, R. Vasseur, M. P. A. Fisher, and A. W. W. Ludwig, Statistical mechanics model for Clifford random tensor networks and monitored quantum circuits, [arXiv:2110.02988](https://arxiv.org/abs/2110.02988) [cond-mat.stat-mech] (2021).
- [62] O. Lunt, J. Richter, and A. Pal, in *Entanglement in Spin Chains: From Theory to Quantum Technology Applications*, edited by A. Bayat, S. Bose, and H. Johannesson (Springer International Publishing, Cham, 2022), p. 251 (specific prepublication chapter <https://arxiv.org/abs/2112.06682>).
- [63] D. Gottesman, The Heisenberg representation of quantum computers, [arXiv:quant-ph/9807006](https://arxiv.org/abs/quant-ph/9807006) [quant-ph] (1998).
- [64] S. Aaronson and D. Gottesman, Improved simulation of stabilizer circuits, *Phys. Rev. A* **70**, 052328 (2004).
- [65] A. W. Harrow and R. A. Low, Random quantum circuits are approximate 2-designs, *Commun. Math. Phys.* **291**, 257 (2009).
- [66] Z. Webb, The Clifford group forms a unitary 3-design, *Quantum Inf. Comput.* **16**, 1379 (2016).
- [67] H. Zhu, Multiqubit Clifford groups are unitary 3-designs, *Phys. Rev. A* **96**, 062336 (2017).
- [68] B. Derrida and D. Stauffer, Phase transitions in two-dimensional Kauffman cellular automata, *Europhys. Lett.* **2**, 739 (1986).
- [69] S.-W. Liu, J. Willsher, T. Bilitewski, J.-J. Li, A. Smith, K. Christensen, R. Moessner, and J. Knolle, Butterfly effect and spatial structure of information spreading in a chaotic cellular automaton, *Phys. Rev. B* **103**, 094109 (2021).
- [70] E. Abrahams, P. W. Anderson, D. C. Licciardello, and T. V. Ramakrishnan, Scaling Theory of Localization: Absence of Quantum Diffusion in Two Dimensions, *Phys. Rev. Lett.* **42**, 673 (1979).
- [71] P. A. Lee and T. V. Ramakrishnan, Disordered electronic systems, *Rev. Mod. Phys.* **57**, 287 (1985).
- [72] F. Evers and A. D. Mirlin, Anderson transitions, *Rev. Mod. Phys.* **80**, 1355 (2008).
- [73] T. Farrelly, A review of quantum cellular automata, *Quantum* **4**, 368 (2020).
- [74] J. Gütschow, S. Uphoff, R. F. Werner, and Z. Zimborás, Time asymptotics and entanglement generation of Clifford quantum cellular automata, *J. Math. Phys.* **51**, 015203 (2010).
- [75] D.-M. Schlingemann, H. Vogts, and R. F. Werner, On the structure of Clifford quantum cellular automata, *J. Math. Phys.* **49**, 112104 (2008).
- [76] M. A. Nielsen and I. L. Chuang, *Quantum Computation and Quantum Information: 10th Anniversary Edition* (Cambridge University Press, 2010).
- [77] A. Chandran and C. R. Laumann, Semiclassical limit for the many-body localization transition, *Phys. Rev. B* **92**, 024301 (2015).
- [78] R. Koenig and J. A. Smolin, How to efficiently select an arbitrary Clifford group element, *J. Math. Phys.* **55**, 122202 (2014).
- [79] S. Bravyi and D. Maslov, Hadamard-free circuits expose the structure of the Clifford group, *IEEE Trans. Inform. Theory* **67**, 4546 (2021).
- [80] E. van den Berg, A simple method for sampling random Clifford operators, [arXiv:2008.06011](https://arxiv.org/abs/2008.06011) [quant-ph] (2020).
- [81] A. Hama, R. Ionicioiu, and P. Zanardi, Bipartite entanglement and entropic boundary law in lattice spin systems, *Phys. Rev. A* **71**, 022315 (2005).
- [82] D. Fattal, T. S. Cubitt, Y. Yamamoto, S. Bravyi, and I. L. Chuang, Entanglement in the stabilizer formalism, [arXiv:quant-ph/0406168](https://arxiv.org/abs/quant-ph/0406168) [quant-ph] (2004).
- [83] F. Haake, *Quantum Signatures of Chaos* (Springer, 2010), 3rd ed.
- [84] S. Su, Chaos and Measurement-Induced Criticality on Stabiliser Circuits, Senior Thesis, Princeton University (2020), <https://dataspace.princeton.edu/handle/88435/dsp01h989r6258>.
- [85] S. Müller, S. Heusler, P. Braun, F. Haake, and A. Altland, Semiclassical Foundation of Universality in Quantum Chaos, *Phys. Rev. Lett.* **93**, 014103 (2004).
- [86] J. S. Cotler, G. Gur-Ari, M. Hanada, J. Polchinski, P. Saad, S. H. Shenker, D. Stanford, A. Streicher, and M. Tezuka, Black holes and random matrices, *J. High Energy Phys.* **2017**, 118 (2017).
- [87] H. Gharibyan, M. Hanada, S. H. Shenker, and M. Tezuka, Onset of random matrix behavior in scrambling systems, *J. High Energy Phys.* **2018**, 124 (2018).
- [88] P. Sierant, D. Delande, and J. Zakrzewski, Thouless Time Analysis of Anderson and Many-Body Localization Transitions, *Phys. Rev. Lett.* **124**, 186601 (2020).
- [89] M. Winer, S.-K. Jian, and B. Swingle, Exponential Ramp in the Quadratic Sachdev-Ye-Kitaev Model, *Phys. Rev. Lett.* **125**, 250602 (2020).

- [90] Y. Liao, A. Vikram, and V. Galitski, Many-Body Level Statistics of Single-Particle Quantum Chaos, *Phys. Rev. Lett.* **125**, 250601 (2020).
- [91] D. Gross, Hudson’s theorem for finite-dimensional quantum systems, *J. Math. Phys.* **47**, 122107 (2006).
- [92] A. Mari and J. Eisert, Positive Wigner Functions Render Classical Simulation of Quantum Computation Efficient, *Phys. Rev. Lett.* **109**, 230503 (2012).
- [93] R. Hudson, When is the Wigner quasi-probability density non-negative?, *Rep. Math. Phys.* **6**, 249 (1974).
- [94] C. Weedbrook, S. Pirandola, R. García-Patrón, N. J. Cerf, T. C. Ralph, J. H. Shapiro, and S. Lloyd, Gaussian quantum information, *Rev. Mod. Phys.* **84**, 621 (2012).
- [95] D. Gross, K. Audenaert, and J. Eisert, Evenly distributed unitaries: On the structure of unitary designs, *J. Math. Phys.* **48**, 052104 (2007).
- [96] H. Zhu, R. Kueng, M. Grassl, and D. Gross, The Clifford group fails gracefully to be a unitary 4-design, [arXiv:1609.08172](https://arxiv.org/abs/1609.08172) [quant-ph] (2016).
- [97] Z. Zimborás, T. Farrelly, S. Farkas, and L. Masanes, Does causal dynamics imply local interactions?, *Quantum* **6**, 748 (2022).
- [98] O. Bratteli and D. Robinson, *Operator Algebras and Quantum Statistical Mechanics 2* (Springer, 2002), 2nd ed.
- [99] B. Dierckx, M. Fannes, and M. Pogorzelska, Fermionic quasifree states and maps in information theory, *J. Math. Phys.* **49**, 032109 (2008).
- [100] P. A. Lee and D. S. Fisher, Anderson Localization in Two Dimensions, *Phys. Rev. Lett.* **47**, 882 (1981).
- [101] A. Harrow and S. Mehraban, Approximate unitary t -designs by short random quantum circuits using nearest-neighbor and long-range gates, *Commun. Math. Phys.* (2023).
- [102] S. Zhou, Z.-C. Yang, A. Hamma, and C. Chamon, Single T gate in a Clifford circuit drives transition to universal entanglement spectrum statistics, *SciPost Phys.* **9**, 87 (2020).
- [103] J. Haferkamp, F. Montealegre-Mora, M. Heinrich, J. Eisert, D. Gross, and I. Roth, Efficient unitary designs with a system-size independent number of non-Clifford gates, *Commun. Math. Phys.* **397**, 995 (2023).
- [104] L. Leone, S. F. E. Oliviero, Y. Zhou, and A. Hamma, Quantum chaos is quantum, *Quantum* **5**, 453 (2021).
- [105] J. Taylor, The Stability of Localisation in Random Time-Periodic Clifford Circuits, Master of Science dissertation, University College London, London (2022).
- [106] A. A. Saberi, Recent advances in percolation theory and its applications, *Phys. Rep.* **578**, 1 (2015).
- [107] R. Durrett, Oriented percolation in two dimensions, *Ann. Probab.* **12**, 999 (1984).